Equivalent-Circuit Models for Split-Ring Resonators and Complementary Split-Ring Resonators Coupled to Planar Transmission Lines

Juan Domingo Baena, Jordi Bonache, Ferran Martín, Ricardo Marqués Sillero, *Member, IEEE*, Francisco Falcone, Txema Lopetegi, *Member, IEEE*, Miguel A. G. Laso, *Member, IEEE*, Joan García–García, Ignacio Gil, Maria Flores Portillo, and Mario Sorolla, *Senior Member, IEEE*

***Abstract*—In this paper, a new approach for the development of planar metamaterial structures is developed. For this purpose, split-ring resonators (SRRs) and complementary split-ring resonators (CSRRs) coupled to planar transmission lines are investigated. The electromagnetic behavior of these elements, as well as their coupling to the host transmission line, are studied, and analytical equivalent-circuit models are proposed for the isolated and coupled SRRs/CSRRs. From these models, the stopband/passband characteristics of the analyzed SRR/CSRR loaded transmission lines are derived. It is shown that, in the long wavelength limit, these stopbands/passbands can be interpreted as due to the presence of negative/positive values for the effective ε and μ of the line. The proposed analysis is of interest in the design of compact microwave devices based on the metamaterial concept.**

***Index Terms*—Duality, metamaterials, microwave filters, split-ring resonators (SRRs).**

I. Introduction

In RECENT years, there has been a growing interest for the design of one-, two-, and three-dimensional artificial structures (also called metamaterials) with electromagnetic properties generally not found in nature. Among them, special attention has been devoted to double-negative media. These are artificial periodic structures composed of sub-wavelength constituent elements that make the structure behave as an effective medium with negative values of permittivity (ε) and permeability (μ) at the frequencies of interest. The properties of such media were already studied by Veselago [1] over 30 years ago. Due to the simultaneous negative values of ε and μ, the wave vector $\mathbf{k}$ and the vectors $\mathbf{E}$ and $\mathbf{H}$ (the electric- and magnetic-field intensity) form a left-handed triplet, with the result of antiparallel phase and group velocities, or backward-wave propagation. Due to left-handedness, exotic electromagnetic properties are expected for left-handed metamaterials (LHMs); namely, inversion of the Snell law, inversion of the Doppler effect, and backward Cherenkov radiation. It is also worth mentioning the controversy originated four years ago from the paper published by Pendry [2], where amplification of evanescent waves in LHMs is pointed out [3]–[6].

In spite of these interesting properties, it was not until 2000 that the first experimental evidence of left-handedness was demonstrated [7]. Following this seminal paper, other artificially fabricated structures exhibiting a left-handed behavior were reported [8]–[11] including the experimental demonstration of negative refraction [12]–[14] and backward wave radiation [15]. The original medium proposed in [7] consists of a bulky combination of metal wires and split-ring resonators (SRRs) [16] disposed in alternating arrows. However, SRRs are actually planar structures, and wires can be easily substituted by metallic strips [8]. Therefore, the extension of these designs to planar configurations can be envisaged [17], [18], thus, opening the way to new planar microwave devices. In fact, in coplanar waveguide (CPW) technology, miniaturized stopband [19] and bandpass filters [20] have been recently reported by some of the authors. In these implementations, SRRs are etched in the back substrate side, underneath the slots, to achieve high magnetic coupling between line and rings at resonance. The presence of the rings leads to an effective negative-valued permeability in a narrow band above resonance, where signal propagation is inhibited. By simply adding shunt metallic strips between the central strip and ground planes, the authors have demonstrated the switch to a bandpass characteristic [18], [20]. This effect has been interpreted as due to the coexistence of effective negative permeability and permittivity (the latter introduced by the additional strips) [18].

In microstrip technology, SRRs etched in the upper substrate side, in proximity to the conductor strip, have been found to provide similar effects [21]. Broad-band negative-μ media in microstrip technology can also be fabricated by periodically etching series gaps in the conductor strip [11], [22]–[26]. However, the implementation of an associated effective negative ε requires the use of shunt inductances, which are associated to metallic vias to the ground [11], [22]–[26]. Now, a key question arises: is it possible to conceive the dual counterpart of SRRs? If so, an effective negative permittivity could be introduced in microstrip devices by using this concept. In a recent paper [27], it was demonstrated by some of the authors that by periodically

Manuscript received June 1, 2004; revised October 20, 2004. This work was supported by the Dirección General de Investigación and the Comisión Interministerial de Ciencia y Tecnología under Contract TIC2002-04528-C02-01, Contract TEC2004-04249-C02-01, Contract TEC2004-04249-C02-02, and Contract PROFIT-070000-2003-933.

J. D. Baena and R. Marqués Sillero are with the Departamento de Electrónica y Electromagnetismo, Universidad de Sevilla, 41012 Seville, Spain.

J. Bonache, F. Martín, J. García–García, and I. Gil are with the Departament d'Enginyeria Electrònica, Universitat Autònoma de Barcelona, 08193 Bellaterra (Barcelona), Spain

F. Falcone, T. Lopetegi, M. A. G. Laso, M. Flores Portillo, and M. Sorolla are with the Electrical and Electronic Engineering Department, Public University of Navarre, E-31006 Pamplona, Spain.

Digital Object Identifier 10.1109/TMTT.2005.845211

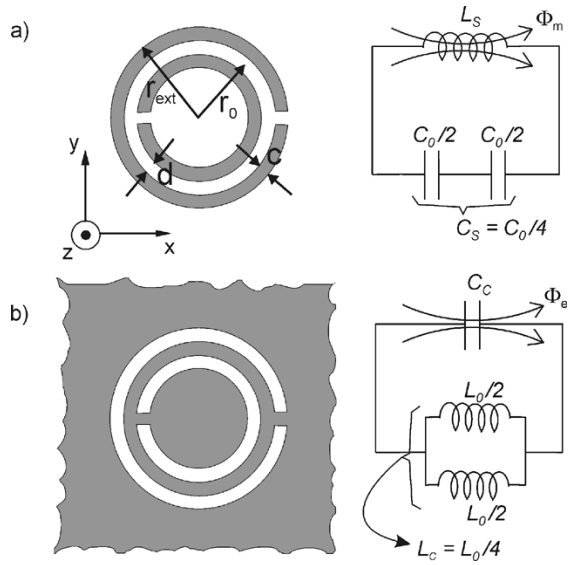

Fig. 1. Topologies of the: (a) SRR and (b) CSRR, and their equivalent-circuit models (ohmic losses can be taken into account by including a series resistance in the model). Grey zones represent the metallization.

etching the *negative image* of SRRs in the ground plane of a microstrip line underneath the conductor strip, a narrow stopband appeared at approximately the resonant frequency of a conventional SRR of identical dimensions etched on the same substrate. The stopband characteristic obtained in the above-cited structure was interpreted as due to a negative effective permittivity introduced by these new elements, electrically coupled to the host transmission line. For the reasons that will be explained in Section II, these new elements have been termed as complementary split-ring resonators (CSRRs) (see Fig. 1). More recently, it has been shown that, by periodically etching capacitive gaps along the aforementioned CSRR-loaded microstrip line, the reported stopband switches to a passband [28], [29]. This effect has been interpreted as due to a left-handed behavior of the line.

In summary, by properly coupling SRRs and/or CSRRs to a host planar transmission line (CPW or microstrip), planar structures with effective negative constituent parameters can be obtained. By adding shunt strips and/or capacitive gaps, a left-handed behavior is achieved. These structures are fully planar (i.e., without vias or other no-planar objects) and can be easily fabricated by using standard photo-etching techniques. The main purpose of this paper is to provide a simple and analytical technique for the design of these structures. This technique is based on lumped-element circuit models, able to describe the elements and their coupling to the host transmission lines, as well as on analytical formulas to determine the main circuit parameters for these models. As a consequence of this analytical approach, the proposed circuit models can be directly programmed and run in a PC station with negligible computation time. Therefore, the proposed approach can provide useful *ab initio* calculations on the physical behavior of the analyzed structures. Although today almost all microwave designers are equipped with useful simulation tools, able to analyze the studied structures, such an approach to the design could be time consuming and blind. Therefore, we feel that the analytical tools presented in this paper will be useful for numerous workers in the field, at least as a first approach to the design (of course, conventional commercial simulation tools will also take a place in this approach as a second-order approximation and fine-tuning tools). Comparison between the frequency responses provided by the proposed analytical circuit models and those experimentally obtained from fabricated SRR- and CSRR-loaded planar transmission lines are also provided in this paper. A satisfactory agreement between the proposed analytical models and reported experimental results is shown in all cases.

II. Electromagnetic Behavior of SRRs and CSRRs

A. Physics of SRRs and CSRRs and Its Equivalent-Circuit Models

The electromagnetic properties of SRRs have been already analyzed in [30] and [31]. This analysis shows that SRRs behave as an LC resonator that can be excited by an external magnetic flux, exhibiting a strong diamagnetism above their first resonance. SRRs also exhibit cross-polarization effects (magnetoelectric coupling) [31] so that excitation by a properly polarized time-varying external electric field is also possible. Fig. 1 shows the basic topology of the SRR, as well as the equivalent-circuit model proposed in [30]. In this figure, C_o stands for the total capacitance between the rings, i.e., $C_o = 2\pi r_o C_{\rm pul}$, where $C_{\rm pul}$ is the per unit length capacitance between the rings. The resonance frequency of the SRR is given by $f_o = (L_s C_s)^{-1/2}/2\pi$, where C_s is the series capacitance of the upper and lower halves of the SRR, i.e., $C_s = C_o/4$. The inductance L_s can be approximated by that of a single ring with *averaged* radius r_o and width c [30].

If the effects of the metal thickness and losses, as well as those of the dielectric substrate are neglected, a perfectly dual behavior is expected for the complementary screen of the SRR [28]. Thus, whereas the SRR can be mainly considered as a resonant magnetic dipole that can be excited by an axial magnetic field [30], the CSRR (Fig. 1) essentially behaves as an electric dipole (with the same frequency of resonance) that can be excited by an axial electric field. In a more rigorous analysis, the cross-polarization effects in the SRR [30], [31] should be considered and also extended to the CSRR. Thus, this last element will also exhibit a resonant magnetic polarizability along its y-axis (see Fig. 1) and, therefore, its main resonance can also be excited by an external magnetic field applied along this direction [28]. These features do not affect the intrinsic circuit model of the elements, although they may affect its excitation model. The intrinsic circuit model for the CSRR (dual of the SRR model) is also shown in Fig. 1. In this circuit [32], the inductance L_s of the SRR model is substituted by the capacitance C_c of a disk of radius $r_o - c/2$ surrounded by a ground plane at a distance c of its edge. Conversely, the series connection of the two capacitances $C_0/2$ in the SRR model is substituted by the parallel combination of the two inductances connecting the inner disk to the ground. Each inductance is given by $L_o/2$, where $L_o = 2\pi r_o L_{\rm pul}$ and $L_{\rm pul}$ is the per unit length inductance of the CPWs connecting the inner disk to the ground. For infinitely thin perfect conducting screens, and in the absence of any dielectric substrate, it directly follows from duality that the parameters of the circuit models for the SRRs and CSRRs are related by $C_c = 4(\varepsilon_o/\mu_o)L_s$ and $C_0 = 4(\varepsilon_o/\mu_o)L_0$. The factor

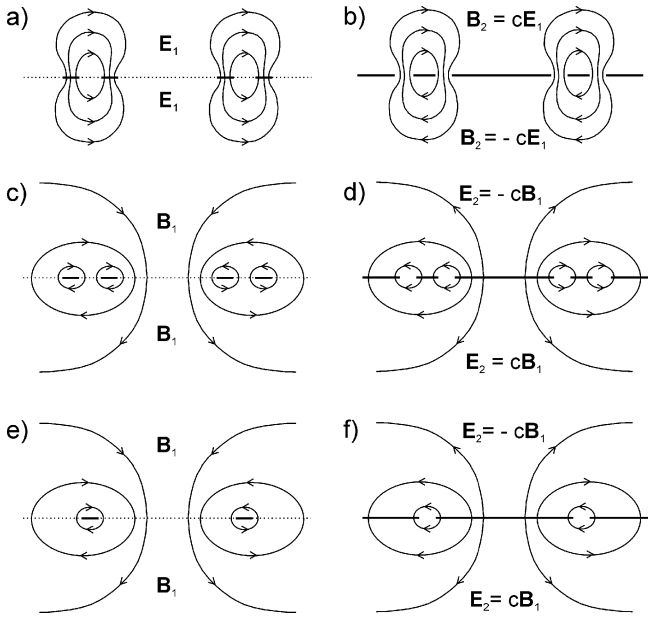

Fig. 2. Sketch of the electric- and magnetic-field lines in the SRR (left-hand side) and the CSRR (right-hand side). (a) Electric-field lines in the SRR at resonance. (b) Magnetic-field lines in the dual CSRR. (c) and (d) Magnetic- and electric-field lines in the SRR and CSRR, respectively. (e) Magnetic induction field in the equivalent ring inductance used for the computation of L_s in the SRR [27]. (f) Electric field in the dual equivalent capacitor proposed for the computation of C_c for the CSRR.

of 4 appearing in these relations is deduced from the different symmetry properties of the electric and magnetic fields of both elements, as is sketched in Fig. 2. From the above relations, it is easily deduced that the frequency of resonance of both structures is the same, as is expected from duality.

The proposed analysis can be easily extended to other planar topologies derived from the basic geometry of the SRR [33]. Some examples are shown in Fig. 2. It is worth noting that some of these topologies do not exhibit cross-polarization effects and, hence, these effects are also absent in their complementary counterparts. The proposed equivalent circuits for these topologies, as well as for their complementary configurations, are also shown in this figure. The nonbianisotropic split-ring resonator (NB SRR) is a slight modification of the basic SRR topology, which shows a 180° rotation symmetry in the plane of the element. As a consequence of this symmetry, cross-polarization effects are not possible in the NB SRR. However, the equivalent-circuit model and resonant frequency of the NB SRR are identical to those of the SRR. The double-slit SRR (D SSR) also presents the aforementioned symmetry, thus avoiding cross polarization. However, the D-SSR equivalent circuit differs from that of the SRR, being the frequency of resonance twice than that of the SRR (of identical size). Finally, the spiral resonator (SR) [34], as well as the double spiral resonator (DSR) [32] allows for a reduction of the resonant frequency with respect to the SRR, as can be seen from its proposed equivalent circuits.

It has been already mentioned that the behavior of SRRs and CSRRs (as well as their derived geometries) are strictly dual for perfectly conducting and infinitely thin metallic screens placed in vacuum. However, deviations from duality—which may give rise to a shift in the frequencies of resonance—arise from losses,

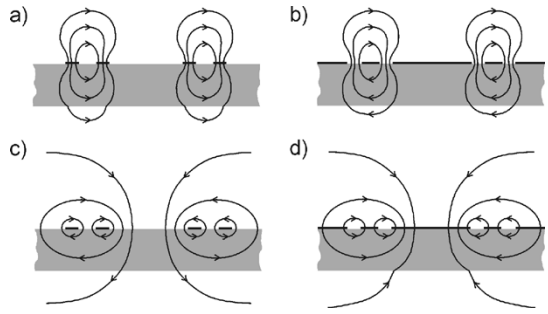

Fig. 3. Sketch of the: (a) electric- and (c) magnetic-field lines of an SRR on a dielectric substrate. (b) Magnetic- and (d) electric-field lines of a similar CSRR on the same dielectric substrate are also sketched.

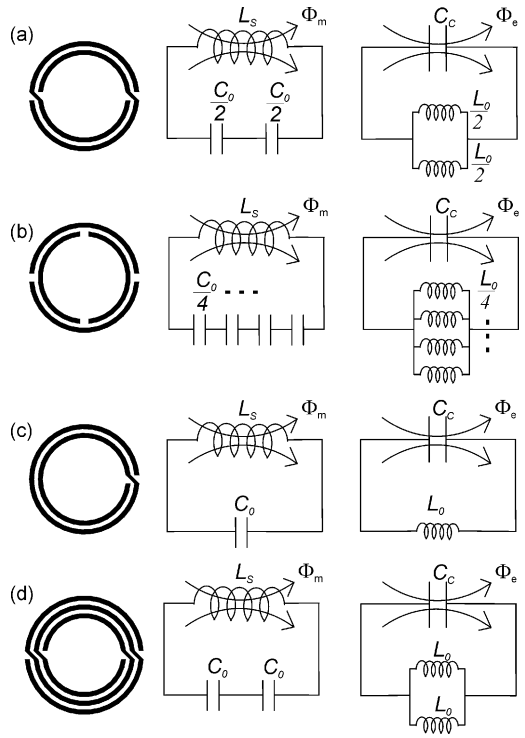

Fig. 4. Topologies corresponding to: (a) the NB SRR, (b) the D SRR, (c) the SR, and (d) the DSR. The equivalent circuits for these topologies are depicted in the second column, while the circuits models for the complementary counterparts are represented in the third column.

finite width of metallizations, and the presence of a dielectric substrate. The latter is expected to be the main cause of deviations from duality. This fact is due to the variations of the elements of the CSRR circuit model, C_c and L_o, from the values extracted from the SRR circuit model parameters C_o and L_s by duality ($C_c = 4(\varepsilon_o/\mu_o)L_s$, and $C_0 = 4(\varepsilon_o/\mu_o)L_0$). As is sketched in Fig. 3, these variations arise directly from the presence of a dielectric substrate, which affects C_c and C_o, but leave L_s and L_o unaltered. Similar deviations from duality arise in the derived topologies shown in Fig. 2.

Analytical expressions for L_s and C_0 in the SRR when a dielectric substrate is present were provided in [30]. As we have already mentioned, the capacitance C_c in Figs. 1 and 4 is that corresponding to a metallic disk of radius $r_o - c/2$ surrounded by a ground plane at a distance c (see Fig. 1). An analytical approximate expression for C_c when a dielectric substrate is

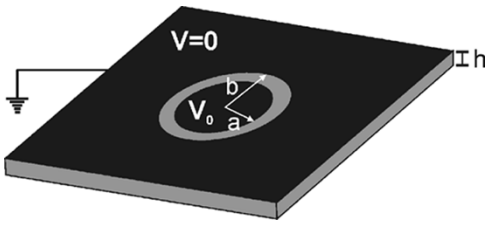

Fig. 5. Capacitance of the CSRR is approximately equal to that corresponding to a metallic disk of radius $a = r_0 - c/2$ surrounded by a ground plane at a distance $b - a = c$, being r_0, the averaged radius of the CSRR, and c, the width of the slots in this. The dielectric substrate is characterized by its permittivity ε and thickness h.

present (see Fig. 5) is derived in the Appendix . The final expression is

$$C_c = \frac{\pi^3 \varepsilon_0}{c^2} \times \int_0^{+\infty} dk \frac{\left[b\mathcal{B}(kb) - a\mathcal{B}(ka)\right]^2}{k^2} \left[\frac{1}{2}\left(1 + \frac{1 + \frac{\varepsilon}{\varepsilon_0}\, tgh(kh)}{1 + \frac{\varepsilon_0}{\varepsilon}\, tgh(kh)}\right)\right] \quad (1)$$

where the meaning of the different symbols is explained in the Appendix.

The inductance L_o in Figs. 1 and 4 is that corresponding to a circular CPW structure of length $2\pi r_o$, strip width d, and slot width c. For the present purposes, the design formulas given in [35] for the per unit length CPW inductance provide enough accuracy and have been used in all numerical computations throughout this study.

B. Numerical Calculations and Experimental Validation

The effect of the dielectric substrate in the frequency of resonance of the CSRR and SRR is shown in Fig. 6. As is expected, there is no difference for the two limiting values of a zero and an infinite substrate thickness. However, significant differences in the values of the frequency of resonance for both elements can be observed for intermediate thicknesses.

The accuracy of the circuit models for the SRR and its derived geometries (see Figs. 1 and 4) has been already experimentally checked in some previous papers [30], [33], [34]. In order to experimentally verify the accuracy of the proposed circuit models for the CSRR and derived geometries, a set of these resonators with different topologies were etched on a metallized microwave substrate and its frequencies of resonance were measured. Their dual counterparts were also manufactured and measured for completeness. The resonant frequencies were obtained from the transmission coefficient S_{21}, measured in a rectangular waveguide, properly loaded with the corresponding element [32]. The waveguide was excited in the fundamental TE_{01} mode and connected to an Agilent 8510 network analyzer. The SRRs or derived geometries were placed in the central E-plane so that they were excited by the magnetic field perpendicular to the element plane. Their dual counterparts were etched in the top wall of the waveguide, being excited by the electric field perpendicular to the element plane. Fig. 7 shows the transmission coefficients for an SRR and an NB SRR with identical geometrical parameters, as well as the same coefficients for its duals [CSRR and complimentary NB SRR (C-NB SRR)]. It can be

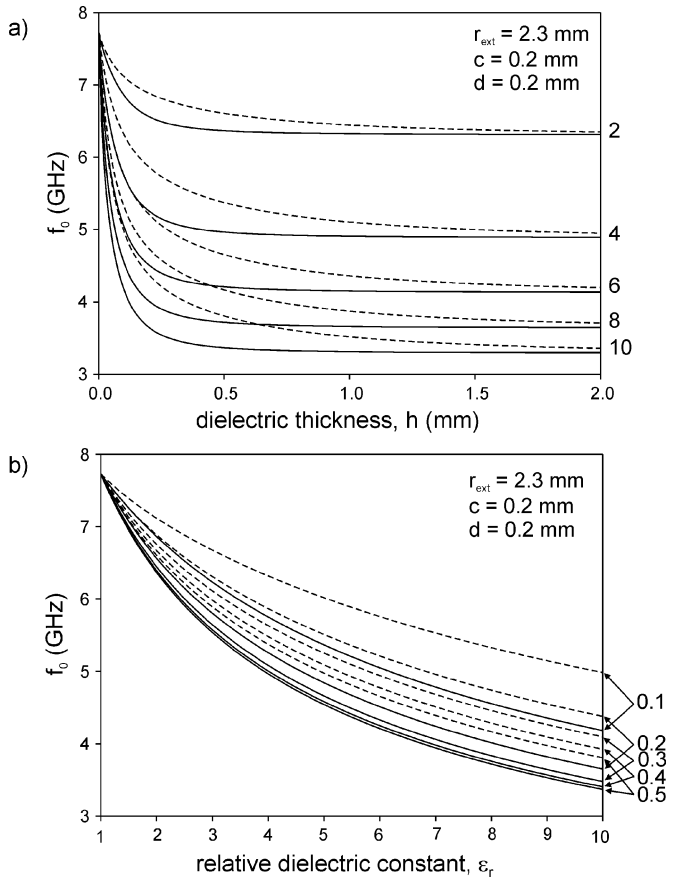

Fig. 6. Numerical calculations showing the dependence of the resonant frequency of SRRs (solid lines) and CSRRs (dashed lines) on the substrate parameters. (a) Dependence on the dielectric thickness for different values of the relative permittivity of the substrate (shown at right). (b) Dependence on the value of the relative dielectric constant for different substrate thickness (in millimeters).

easily seen that the SRR and NB SRR have the same frequency of resonance (the small shift can be attributed to tolerances in the manufacturing process). The same can be said for its complementary elements. Fig. 8 illustrates the cross-polarization effects in the SRR, as well as the absence of these effects in the NB SRR (this last element is not excited in positions 3 and 4), as is predicted by the theory [33]. This figure also shows that the magnetic excitation is by far the most efficient for the SRR. From duality, it can be deduced that the electric excitation will be the dominant one for the CSRR. Finally, the frequencies of resonance for different configurations, measured following the method illustrated in Fig. 7, are shown in Table I [32]. The theoretical values shown in this table were obtained from the proposed circuit models (see Figs. 1 and 4). As can be seen, a reasonable agreement between theory and experiment was obtained. It is remarkable that the CSRRs always resonate at frequencies slightly higher than those of the SRRs. This effect is sharper for the higher dielectric constants.

III. Lumped-Element Circuit Models for SRRs and CSRRs Coupled Transmission Lines

Let us now focus on finding the equivalent-circuit models corresponding to transmission-line structures periodically loaded with SRRs or CSRRs. These models should describe the host transmission line, resonators (SRR or CSRRs), and their

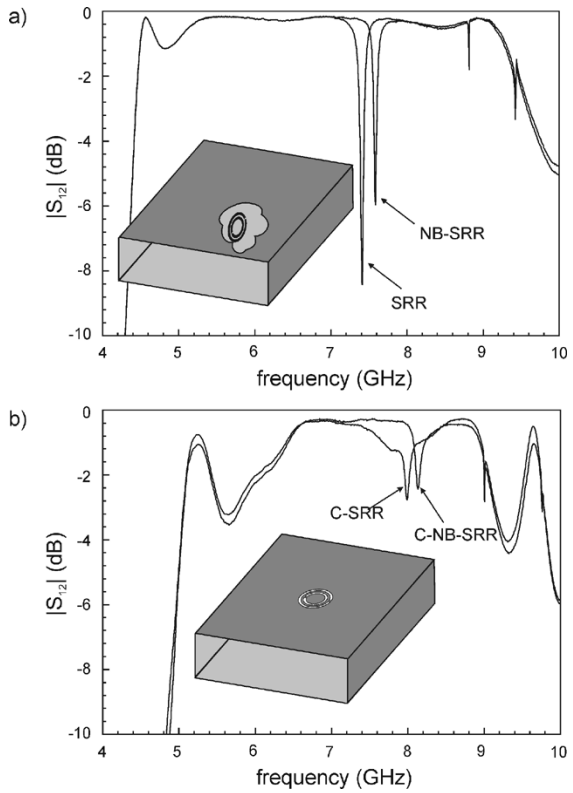

Fig. 7. Frequency response obtained in a rectangular waveguide loaded with SRRs and NB SRRs, as well as its dual counterparts (CSRR and C-NB SRR). The method of excitation is sketched in the inset of this figure. The elements parameters are those of Table I.

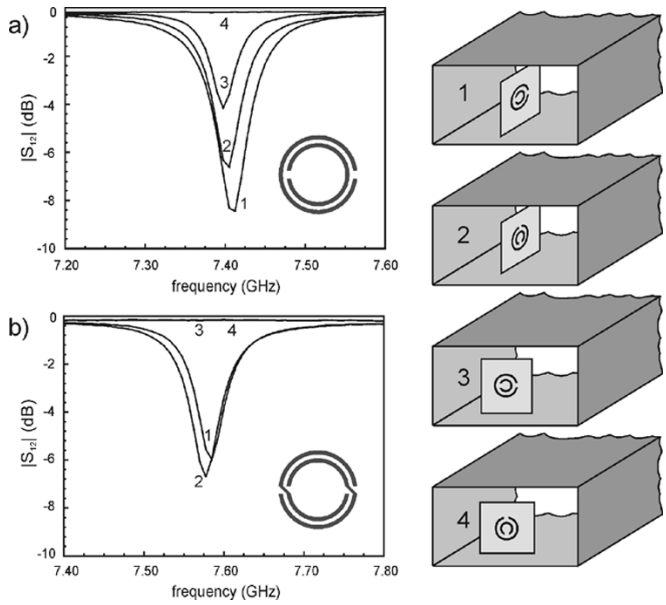

Fig. 8. (a) Experimental demonstration of the cross-polarization effects in the SRR. Position 1: electric and magnetic excitation. Position 2: only magnetic excitation. Position 3: only electric excitation. Position 4: no excitation. The behavior of the NB SRR under the same excitations is shown in (b). The absence of electric excitation (3 and 4) shows the absence of cross-polarization effects at resonance.

coupling. It has been indicated that the basic SRR and CSRR topologies (Fig. 1) exhibit cross-polarization effects. This means that both SRRs and CSRRs can be magnetically and/or

TABLE I
MEASURED AND THEORETICAL VALUES FOR THE FREQUENCY OF RESONANCE. THE RESONATORS ARE PRINTED ON A SUBSTRATE WITH THICKNESS $t = 0.49$ mm AND RELATIVE PERMITTIVITY $\varepsilon_r = 2.43$. THE PARAMETERS OF RINGS, NAMED JUST AS IN FIG. 1, ARE $^{(1)}$ $r_0 = 1.7$ mm, $c = d = 0.2$ mm; $^{(2)}$ $r_0 = 3.55$ mm, $c = d = 0.3$ mm

	Conventional		Complementary	
	f_0^{th} (GHz)	f_0^{exp} (GHz)	f_0^{th} (GHz)	f_0^{exp} (GHz)
SRR[1]	7.17	7.40	7.49	8.00
NB-SRR[1]	7.17	7.56	7.49	8.14
DSR[1]	5.07	5.05	5.30	5.49
SR2[1]	3.59	3.78	3.75	4.07
SRR[2]	3.33	3.40	3.56	3.77
DSRR[2]	6.66	6.77	7.12	7.41

electrically excited if the rings are properly oriented. However, it has been verified (see Fig. 8) that magnetic/electric coupling are the dominant coupling mechanisms in SRRs/CSRRs. Therefore, cross-polarizations effects can be ignored in a first-order approximation (this assumption will be strictly valid for NB SRRs and other nonbianisotropic configurations). As discussed in Section II, to properly excite SRRs by means of a time-varying magnetic field, a significant component in the axial direction is required. This makes the CPW structure the preferred host transmission line for SRRs excitation. It was previously shown by the authors [18]–[20] that by etching the SRRs in the back substrate side, underneath the slots, high magnetic coupling is achieved. Alternatively, SRRs can be etched in the upper substrate side, between signal and ground, but this requires very wide slots to accommodate the rings and produces significant mismatch [36]. In contrast, since CSRRs require electric coupling, with a significant component of the electric field perpendicular to the CSRRs surface, microstrip lines with rings etched in the ground plane (below the conductor strip) are more convenient [27], [28]. This do not mean that CPW structures should be ruled out, although electric coupling to CSRRs is softer (in comparison to microstrip) and rejection in the vicinity of the resonant frequency is degraded.

Due to the small electrical dimensions of SRRs and CSRRs at resonance, the structures (CPW or microstrip loaded lines) can be described by means of lumped-element equivalent circuits. For the SRR loaded transmission line, the proposed equivalent-circuit model is shown in Fig. 9(a) [18], [19]. L and C are the per-section inductance and capacitance of the line, while the SRRs are modeled as a resonant tank (with inductance L_s and capacitance C_s) magnetically coupled to the line through a mutual inductance, M. Due to the symmetry of the structure, the magnetic wall concept has been used and the circuit shown in Fig. 9(a) actually corresponds to one-half of the basic cell. The equivalent impedance of the series branch can be simplified to that shown in the circuit of Fig. 9(b) [18], which is formally identical to the series impedance corresponding to a left-handed transmission line [23]–[26] (in that region where the total series impedance is capacitive). From the circuit of Fig. 9(b), the dispersion relation can be easily obtained as follows:

$$\cos(\beta l) = 1 - \frac{LC\omega^2}{2} + \frac{\dfrac{C}{C_s'}}{4\left(1 - \dfrac{\omega_o^2}{\omega^2}\right)} \tag{2}$$

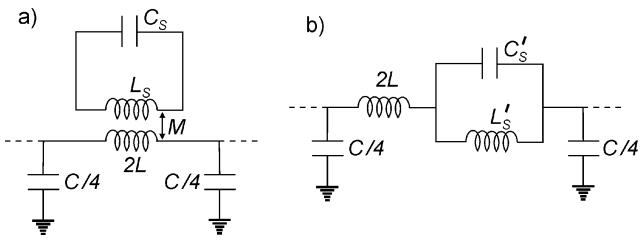

Fig. 9. (a) Lumped-element equivalent circuit for the basic cell of the SRR loaded transmission line. (b) Simplified circuit with the series branch replaced by its equivalent impedance.

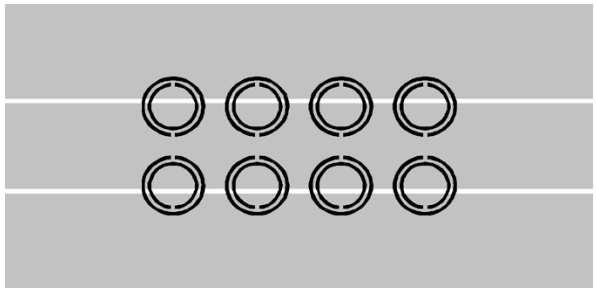

Fig. 10. Layout of the fabricated SRR loaded CPW structure drawn to scale. SRR dimensions: $c = d = 0.2$ mm and $r_{\rm ext} = 1.9$ mm. Adjacent ring pairs are separated 5 mm. The strip and slots widths ($W = 5.4$ mm and $G = 0.3$ mm) have been determined to achieve a 50-Ω line. The structure has been fabricated on an Arlon 250-LX-0193-43-11 substrate with thickness $h = 0.49$ mm and dielectric constant $\varepsilon_r = 2.43$. Actual device length (including access lines) is 35 mm.

with $C_s' = L_s/(M^2\omega_o^2)$, $L_s' = C_s M^2 \omega_o^2$, and $\omega_o^2 = 1/(L_s C_s) = 1/(L_s' C_s')$. β is the propagation constant for Bloch waves and l is the period of the structure. For an SRR-loaded CPW structure, line parameters (L and C) can be determined from a transmission-line calculator, L_s and C_s from the aforementioned SRR circuit model, and M can be inferred from the fraction f of the slot area occupied by the rings according to

$$M = 2L \cdot f. \tag{3}$$

These circuit elements have been calculated for the structure shown in Fig. 10 (a CPW with pairs of SRRs etched in the back substrate side). The dispersion relation for the corresponding infinite periodic structure is depicted in an ω–β diagram in Fig. 11. A frequency gap around the theoretical frequency of resonance of the rings ($f_0 = 7.68$ GHz) is observed. The explanation is the following: in a narrow region starting at f_o, the series impedance in Fig. 9(b) becomes negative and signal propagation is inhibited. In contrast, just below the resonance, the series impedance is highly inductive, and makes the second term in (2) positive and higher than unity. The result is a stopband around f_o with a level of rejection that depends on the number of SRR pairs etched in the line.

It was previously reported [18] that the aforementioned stopband can be switched to a passband by periodically inserting metallic strips between the central CPW strip and ground planes (Fig. 12). These additional strips make the structure to behave as a microwave plasma with a negative effective permittivity below the plasma frequency [15]. If this frequency is above the

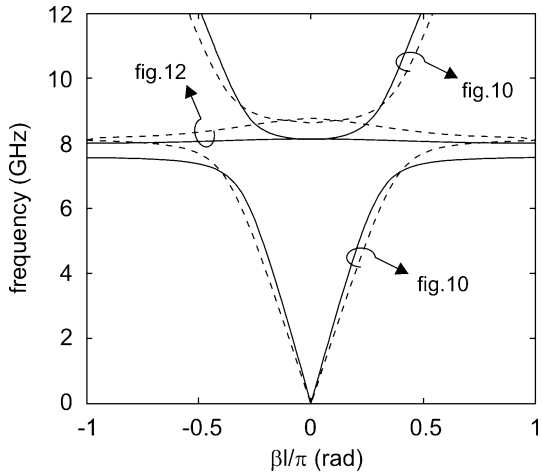

Fig. 11. Theoretical (solid lines) and simulated (dashed lines) dispersion diagram for the infinite periodic SRR–CPW structures with unit cells identical to those shown in Figs. 10 and 12.

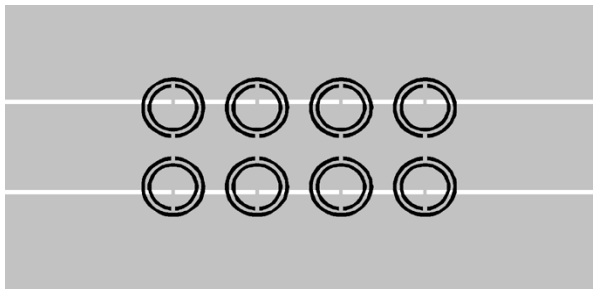

Fig. 12. Layout of the fabricated SRR loaded CPW structure with shunt metal strips, drawn to scale. Dimensions are identical to those of Fig. 10 and the width of the shunt strips is 0.2 mm.

resonant frequency of the SRRs, a narrow passband with backward wave propagation is expected in that region where negative effective permittivity and permeability coexist (i.e., above the resonant frequency of the rings). The strips can be modeled by shunt connected inductances L_p that should be added to the shunt impedance of the circuit of Fig. 9. From this circuit, the dispersion relation can be calculated [18], i.e.,

$$\cos(\beta l) = 1 - \frac{L_p\omega - \dfrac{1}{C\omega}}{\dfrac{4L_p}{C}} \left(2L\omega - \frac{\dfrac{L_s'}{C_s'}}{L_s'\omega - \dfrac{1}{C_s'\omega}} \right) \tag{4}$$

and represented in an ω–β diagram (Fig. 12). In practical computations, L_p can be estimated from the simulated frequency response of the strip-loaded CPW (SRRs removed), where the plasma frequency is given by the resonator composed by C and L_p. A narrow passband is present above the resonant frequency of the SRRs. The propagation constant for Bloch waves (β) decreases with frequency, which is indicative of antiparallel phase and group velocities, and is, therefore, in agreement with the theory. It is worth noting that (4) can be deduced from (2) by simply changing the line capacitance C in (2) by the *effective capacitance* associated to the parallel connection of C and the strip inductance L_p, which is negative below the aforementioned *plasma frequency*. Thus, in the long wavelength limit

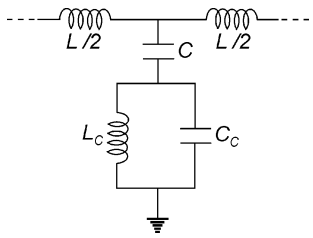

Fig. 13. Lumped-element equivalent circuit for the basic cell of the CSRR loaded microstrip line.

(when βl is very small, i.e., at the upper frequencies), the passband can be associated to the simultaneous presence of a negative series impedance and a negative shunt admittance along the line, i.e., to the simultaneous presence of negative effective ε and μ [24], [26]. It is worth noting that the upper frequency limit of the passband for the structure of Fig. 12 coincides with the lower frequency limit of the stopband for the structure in Fig. 10. This fact is consistent with the aforementioned interpretation: in the long wavelength limit, the structure of Fig. 10 presents an effective negative μ and an effective positive ε.

The dispersion diagrams, computed from electromagnetic simulations (using the Agilent Momentum commercial software) are also shown in Fig. 11. In agreement with the theory, both the theoretical and simulated passbands for the structure of Fig. 12 are located inside the corresponding stopbands for the structure of Fig. 10, and the upper limit of the passband for the structure in Fig. 12 coincides with the lower limit of the upper stopband for the structure in Fig. 10. There is a small shift in frequency between theory and simulations, which is usual in this kind of resonant structures [7].

Let us now analyze the CSRR loaded transmission lines. Since CSRRs are etched in the ground plane, and they are mainly excited by the electric field induced by the line, this coupling can be modeled by series connecting the line capacitance to the CSRRs. According to this, the proposed lumped-element equivalent circuit for the CSRR loaded transmission line is that depicted in Fig. 13.

Again, L and C are the per-section inductance and capacitance of the line, while L_c and C_c model the CSRR, as has been previously shown. From the circuit of Fig. 13, the dispersion relation can be obtained by simple calculation as follows:

$$\cos(\beta l) = 1 + \frac{L}{2\left(\dfrac{L_c}{1-\dfrac{\omega^2}{\omega_o^2}} - \dfrac{1}{C\omega^2}\right)} \tag{5}$$

where $\omega_o = 2\pi f_o = (L_c C_c)^{-1/2}$ is the angular resonant frequency of the CSRRs. Inspection of (5) points out the presence of a frequency gap in the vicinity of f_o. This is confirmed by the theoretical dispersion relation (see Fig. 14) corresponding to the structure depicted in Fig. 15, a 50-Ω microstrip line with CSRRs etched in the back side metal (ground plane) [25]. In theoretical calculations, L and C have been inferred from a transmission-line calculator, while L_c and C_c have been obtained according to the model described in Section II. In the frequency interval delimited by f_o (upper limit) and $f_c = [L_s(C_s + C)]^{-1/2}/2\pi$ (lower limit), the shunt impedance is dominated by the tank inductance, and the structure behaves as a one-dimensional effective medium with negative permittivity. Therefore, propagating modes are precluded in this frequency band. When the discrete nature of the structure is explicitly taken into account, it is realized that the rejection band should extend slightly below f_c due to the extreme values of the shunt admittance in a narrow band below this frequency.

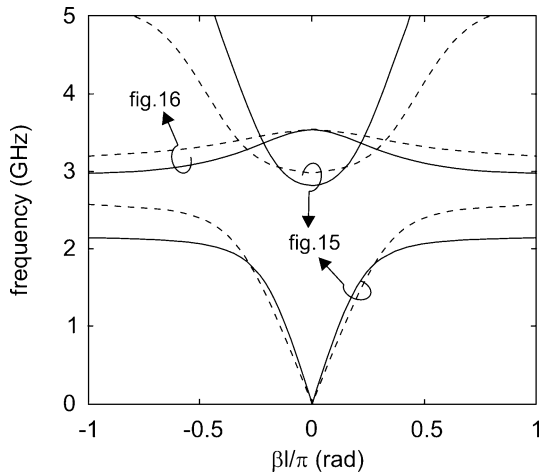

Fig. 14. Theoretical (solid lines) and simulated (dashed lines) dispersion diagram for the infinite CSRR- microstrip structures with unit cells identical to those shown in Figs. 15 and 16. The mismatch between the stopbands and passbands is due to the different dimensions of the CSRRs in Figs. 15 and 16.

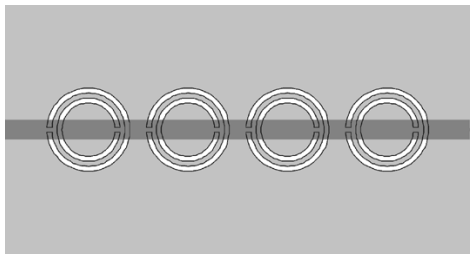

Fig. 15. Layout of a 50-Ω microstrip line with CSRRs etched on the back substrate side. Dielectric substrate is Rogers RO3010 ($h = 1.27$ mm, $\varepsilon_r = 10.2$). CSRR dimensions are $c = d = 0.3$ mm, $r_{\text{ext}} = 3.0$ mm and the periodicity is 7 mm. The conductor strip has a width of $W = 1.2$ mm corresponding to a characteristic impedance of 50 Ω.

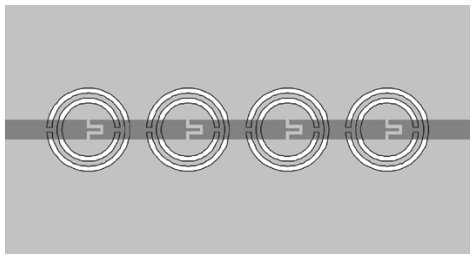

Fig. 16. Layout of a 50-Ω microstrip line with CSRRs etched on the back substrate side and series gaps etched in the conductor strip. Dimensions and substrate are as those reported in Fig. 15, except for the external radius of the CSRRs, which has been set to 2.5 mm and periodicity, which is now 6 mm.

In order to obtain a left-handed transmission line based on CSRRs, it is now necessary to introduce an effective negative-valued permeability to the structure. This can be achieved by periodically etching capacitive gaps in the conductor strip at periodic positions (see Fig. 16) [22]–[26]. These gaps provide a

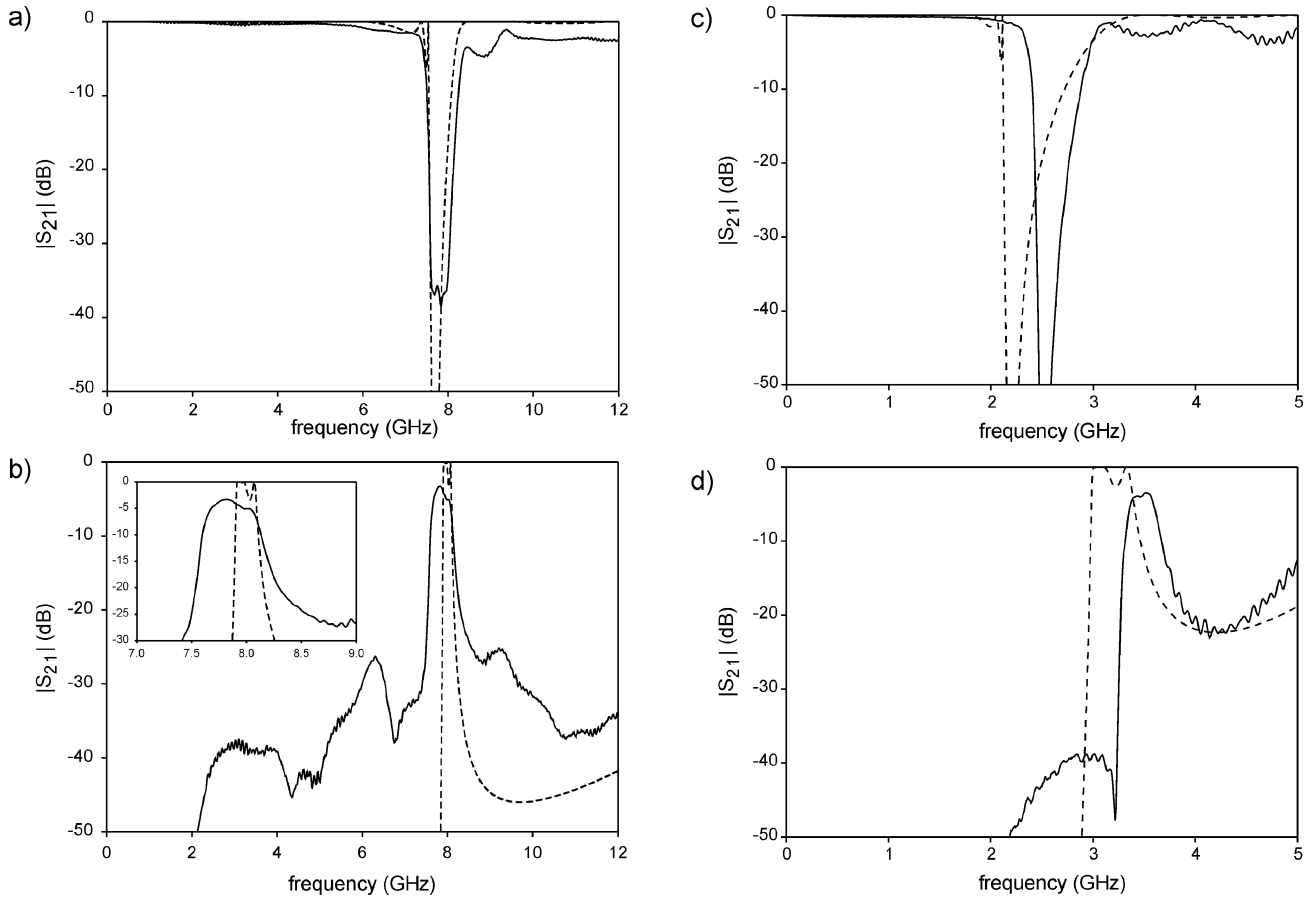

Fig. 17. Insertion loss measured on the fabricated prototypes (solid lines) and results obtained from the equivalent-circuit models (dashed lines). (a) SRR loaded CPW without shunt strips. (b) SRR loaded CPW with shunt strips. (c) CSRR loaded microstrip lines without series gaps. (d) CSRR loaded microstrip lines with series gaps.

negative effective permeability up to a frequency that can be tailored by properly designing the gap dimensions. If this frequency is set above f_o, a narrow left-handed transmission band is expected. The dispersion relation of the CSRR transmission line with series gaps is deduced from the equivalent circuit as

$$\cos(\beta l) = 1 + \frac{L\omega - \dfrac{1}{C_g\omega}}{2\left(\dfrac{L_c\omega}{1 - L_cC_c\omega^2} - \dfrac{1}{C\omega}\right)} \tag{6}$$

where C_g is the gap capacitance. Again, the ω–β representation is indicative of left-handed wave propagation in the allowed band (see Fig. 14). The gap capacitance C_g can be inferred from the cutoff frequency of the structure without CSRRs since this cutoff frequency is given by the frequency of resonance of the resonator formed by the line inductance L and the gap capacitance C_g. The simulated dispersion diagrams for the infinite periodic structures with unit cells identical to those of Figs. 15 and 16 are also shown in Fig. 14. The mismatch between the stopbands and passbands is due to the different periodicity and dimensions of the CSRRs in both structures.

It is worth noting that all the parameters of the proposed equivalent circuits, used in our theoretical computations, have been either inferred from the analytical SRR or CSRR models (L_s, C_s, L_c, and C_c) or estimated from independent physical arguments (M, C, L_p, and C_g). Thus, the reported models are self-consistent and do not rely on any kind of parameter adjustment external to the model.

IV. Comparison With Experimental Data and Discussion

The measured frequency responses for the previous finite size structures (Figs. 10, 12, 15, and 16, respectively) have been measured and the results are shown in Fig. 17 (the Agilent 8722ES vector network analyzer has been used for the measurements). The SRR loaded CPW structures were manufactured on an Arlon 250-LX-0193-43-11 thin dielectric substrate in order to obtain high inductive coupling between line and rings. For the CSRR loaded microstrip lines, a high-permittivity Rogers RO3010 dielectric substrate was used in order to enhance capacitive couplings. The comparison between theoretical and experimental results (see Fig. 17) shows that the proposed circuit models predict the stopbands/passbands with a reasonable accuracy. The bandwidth seems to be better predicted for the microstrip CSRR devices than for the CPW SRR ones. However, the location of the stopbands/passbands is better evaluated in the SRR loaded CPWs than in the CSRR loaded microstrip lines. These results are consistent with the discrepancies and correspondences between theory and simulations reported in Section III. More theoretical and experimental research is needed to explain these discrepancies. However, the agreement between theory and experiments shown in Fig. 17

is actually noticeable. If we mainly take into account that the effects of the coupling between adjacent SRRs or CSRRs, as well as the eventual modification of the SRR/CSRR behavior by the proximity of the line, are not taken into account in the models. This fact seems to confirm that the SRRs and CSRRs behave as almost closed structures, only tightly coupled to the external lines. Finally, in order to evaluate the effect of cross-polarization [31] (not taken into account in the circuit model for the coupling between SRRs/CSRRs and lines), we have simulated the different measured structures, but with the SRRs/CSRRs rotated by 90°. The obtained results (not shown) do not substantially differ from the results shown here. This fact seems to demonstrate that cross-polarization effects can be actually neglected in the analyzed structures, although they are crucial for other devices such as frequency-selective surfaces [28].

V. Conclusions

An analytical procedure for the study of a family of planar structures with negative effective parameters, including left-handed behavior, has been presented in a unified way. The analyzed structures are based on the coupling of SRRs and CSRRs to conventional planar lines. They are fully planar, i.e., they neither incorporate vias, nor other nonplanar inserts, and can be implemented in both CPW and microstrip technology. They can also incorporate modifications of the basic SRR/CSRR geometry. This research has been specifically devoted to obtain analytical tools for the *ab initio* analysis of these structures. To this end, we have first studied the physics of the isolated SRR and CSRR and we have inferred their equivalent-circuit models. The frequencies of resonance obtained from these circuit models have been compared to those obtained experimentally, and a satisfactory agreement has been found. The coupling between planar transmission lines and SRRs/CSRRs has been modeled by means of a mutual inductance and a shunt capacitance, respectively. From the resulting equivalent circuits, the behavior of periodic and finite structures has been inferred. Four structures were considered: two CPW structures coupled to SRRs (with and without shunt metal strips) and two microstrip lines loaded with CSRRs (with and without series gaps). The qualitative behavior of these structures was shown to be in agreement with the previously reported theory of effective media with negative parameters. In addition, the measured frequency responses of these structures was in reasonable quantitative agreement with the theoretical predictions, thus showing the validity of the lumped-element circuit models. This agreement is indicative of the usefulness of the reported circuit models as practical design tools.

Appendix
Variational Calculation of the Capacitive for the CSRR C_c

The capacitance C_c can be obtained from the variational expression

$$U=\frac{1}{2}C_cV_0^2=\frac{1}{2}\iint \rho V dS=\frac{1}{2}\frac{1}{4\pi^2}\int_{-\infty}^{+\infty}dk_x\int_{-\infty}^{+\infty}dk_y\widetilde{\rho}^*\widetilde{V}$$

with a suitable trial function for the electrostatic potential V. For this purpose, we first express the spectral-domain charge density in terms of a suitable Green's function G [35]

$$C_c=\frac{1}{4\pi^2V_0^2}\int_0^{2\pi}d\phi\int_0^{\infty}dkk\frac{\widetilde{V}^*}{\widetilde{G}^*}\widetilde{V}$$

or

$$C_c\le\frac{1}{2\pi}\int_0^{\infty}dkk\frac{\widetilde{u}^*}{\widetilde{G}^*}\widetilde{u}$$

where u is the trial function, which is chosen as

$$u(r)=\begin{cases}1, & \text{if } r<a\\ \dfrac{b-r}{b-a}, & \text{if } a<r<b\\ 0, & \text{if } b<r\end{cases}$$

$$\widetilde{u}(k)=\frac{\pi^2\left(b\mathcal{B}(kb)-a\mathcal{B}(ka)\right)}{k^2\left(b-a\right)}$$

where a and b are the geometrical parameters shown in Fig. 5 and function $\mathcal{B}$ is defined as

$$\mathcal{B}(x)=S_0(x)J_1(x)-S_1(x)J_0(x)$$

with S_n and J_n being the nth-order Struve and Bessel functions. These expressions directly follow (1), which can be easily computed in few steps by using standard integration routines.

Acknowledgment

The authors extend their thanks to Conatel s.l. and Omicron Circuits. The fabricated prototypes presented in this paper are patent pending.

References

[1] V. G. Veselago, "The electrodynamics of substances with simultaneously negative values of ε and μ," *Sov. Phys.—Usp.*, vol. 10, pp. 509–514, 1968.
[2] J. B. Pendry, "Negative refraction makes perfect lens," *Phys. Rev. Lett.*, vol. 85, pp. 3966–3969, 2000.
[3] N. García and M. Nieto-Vesperinas, "Left handed materials do not make perfect lens," *Phys. Rev. Lett.*, vol. 88, pp. 207 403(1)–07 403(4), 2002.
[4] G. Gómez–Santos, "Universal features of the time evolution of evanescent moded in a left handed perfect lens," *Phys. Rev. Lett.*, vol. 90, pp. 077 401(1)–077 401(4), 2003.
[5] D. R. Smith, D. Schurig, M. Rosenbluth, S. Shultz, S. Annanta–Ramakrishna, and J. B. Pendry, "Limitations on subdiffraction imaging with a negative refractive index slab," *Appl. Phys. Lett.*, vol. 82, pp. 1506–1508, 2003.
[6] R. Marqués and J. Baena, "Effect of losses and dispersion on the focusing properties of left handed media," *Microwave Opt. Technol. Lett.*, vol. 41, pp. 290–294, 2004.
[7] D. R. Smith, W. J. Padilla, D. C. Vier, S. C. Nemat-Nasser, and S. Schultz, "Composite medium with simultaneously negative permeability and permittivity," *Phys. Rev. Lett.*, vol. 84, pp. 4184–4187, 2000.
[8] R. A. Shelby, D. R. Smith, S. C. Nemat-Nasser, and S. Schultz, "Microwave transmission through a two-dimensional isotropic left handed metamaterial," *Appl. Phys. Lett.*, vol. 78, pp. 489–491, 2001.
[9] R. Marqués, J. Martel, F. Mesa, and F. Medina, "Left handed media simulation and transmission of EM waves in sub-wavelength SRR-loaded metallic waveguides," *Phys. Rev. Lett.*, vol. 89, pp. 183 901(1)–183 901(4), 2002.
[10] ——, "A new 2D isotropic left handed metamaterial design: Theory and experiment," *Microwave Opt. Technol. Lett.*, vol. 35, pp. 405–408, 2002.

[11] G. V. Eleftheriades, A. K. Iyer, and P. C. Kremer, "Planar negative refractive index media using periodically L–C loaded transmission lines," *IEEE Trans. Microw. Theory Tech.*, vol. 50, no. 12, pp. 2702–2712, Dec. 2002.
[12] R. A. Shelby, D. R. Smith, and S. Schultz, "Experimental verification of a negative index of refraction," *Science*, vol. 292, pp. 77–79, 2001.
[13] C. G. Parazzoli, R. B. Greegor, K. Li, B. E. C. Koltenbah, and M. Tanielian, "Experimental verification and simulation of negative index of refraction using Snell's law," *Phys. Rev. Lett.*, vol. 90, pp. 107 401(1)–07 401(4), 2003.
[14] A. A. Houck, J. B. Brock, and I. L. Chuang, "Experimental observations of a left handed material that obeys Snell's law," *Phys. Rev. Lett.*, vol. 90, pp. 137 401(1)–137 401(4), 2003.
[15] A. Grbic and G. V. Eleftheriades, "Experimental verification of backward wave radiation from a negative refractive index metamaterial," *J. Appl. Phys.*, vol. 92, pp. 5930–5935, 2002.
[16] J. B. Pendry, A. J. Holden, D. J. Robbins, and W. J. Stewart, "Magnetism from conductors and enhanced nonlinear phenomena," *IEEE Trans. Microw. Theory Tech.*, vol. 47, no. 11, pp. 2075–2084, Nov. 1999.
[17] M. Schβüler, A. Fleckenstein, J. Freese, and R. Jakoby, "Lef-handed metamaterials based on split ring resonators for microstrip applications," in *Proc. 33rd Eur. Microwave Conf.*, Munich, 2003, pp. 1119–1122.
[18] F. Martín, F. Falcone, J. Bonache, R. Marqués, and M. Sorolla, "A new split ring resonator based left handed coplanar waveguide," *Appl. Phys. Lett.*, vol. 83, pp. 4652–4654, 2003.
[19] F. Martín, F. Falcone, J. Bonache, T. Lopetegi, R. Marqués, and M. Sorolla, "Miniaturized coplanar waveguide stopband filters based on multiple tuned split ring resonators," *IEEE Microw. Wireless Compon. Lett.*, vol. 13, no. 12, pp. 511–513, Dec. 2003.
[20] F. Falcone, F. Martín, J. Bonache, R. Marqués, T. Lopetegi, and M. Sorolla, "Left handed coplanar waveguide band pass filters based on bi-layer split ring resonators," *IEEE Microw. Wireless Compon. Lett.*, vol. 14, no. 1, pp. 10–12, Jan. 2004.
[21] J. García–García, F. Martín, F. Falcone, J. Bonache, I. Gil, T. Lopetegi, M. A. G. Laso, M. Sorolla, and R. Marqués, "Spurious passband suppression in microstrip coupled line band pass filters by means of split ring resonators," *IEEE Microw. Wireless Compon. Lett.*, vol. 14, no. 9, pp. 416–418, Sep. 2004.
[22] I. H. Lin, C. Caloz, and T. Itoh, "Transmission characteristics of left handed non uniform transmission lines," in *Proc. Asia–Pacific Microwave Conf.*, vol. 3, 19–22, 2002, pp. 1501–1504.
[23] C. Caloz, H. Okabe, H. Iwai, and T. Itoh, "Transmission line approach of left-handed metamaterials," in *Proc. USNC/URSI Nat. Radio Sci. Meeting*, San Antonio, TX, 2002, p. 39.
[24] A. A. Oliner, "A periodic-structure negative-refractive index medium without resonant elements," in *Proc. USNC/URSI Nat. Radio Sci. Meeting*, San Antonio, TX, 2002, p. 41.
[25] O. F. Siddiqui, M. Mojahedi, and G. V. Eleftheriades, "Periodically loaded transmission line with effective negative refractive index and negative group velocity," *IEEE Trans. Antennas Propag.*, vol. 51, no. 10, pp. 2619–2625, Oct. 2003.
[26] G. V. Eleftheriades, O. Siddiqui, and A. Iyer, "Transmission line models for negative refractive index media and associated implementations without excess resonators," *IEEE Microw. Wireless Compon. Lett.*, vol. 13, no. 2, pp. 53–55, Feb. 2003.
[27] F. Falcone, T. Lopetegi, J. D. Baena, R. Marqués, F. Martín, and M. Sorolla, "Effective negative-ε stopband microstrip lines based on complementary split ring resonators," *IEEE Microw. Wireless Compon. Lett.*, vol. 14, no. 6, pp. 280–282, Jun. 2004.
[28] F. Falcone, T. Lopetegi, M. A. G. Laso, J. D. Baena, J. Bonache, M. Beruete, R. Marqués, F. Martín, and M. Sorolla, "Babinet principle applied to metasurface and metamaterial design," *Phys. Rev. Lett.*, vol. 93, pp. 197 401(1)–197 401(4), 2004.
[29] R. Marqués, J. D. Baena, F. Martín, J. Bonache, F. J. Falcone, T. Lopetegi, M. Beruete, and M. Sorolla, "Left-handed metamaterial based on dual split ring resonators in microstrip technology," in *Proc. Int. URSI Electromagnetic Theory Symp.*, Pisa, Italy, May 23–27, 2004, pp. 1188–1190.
[30] R. Marqués, F. Mesa, J. Martel, and F. Medina, "Comparative analysis of edge- and broadside-coupled split ring resonators for metamaterial design—Theory and experiment," *IEEE Trans. Antennas Propag.*, vol. 51, no. 10, pp. 2572–2581, Oct. 2003.
[31] R. Marqués, F. Medina, and R. Rafii-El-Idrissi, "Role of bianisotropy in negative permeability and left handed metamaterials," *Phys. Rev. B, Condens. Matter*, vol. 65, pp. 144 441(1)–144 441(6), 2002.
[32] J. D. Baena, J. Bonache, F. Martín, R. Marqués, F. Falcone, T. Lopetegi, M. Beruete, M. A. G. Laso, J. García–García, F. Medina, and M. Sorolla, "Modified and complementary split ring resonators for metasurface and metamaterial design," in *Proc. 10th Bianisotropics Conf.*, Ghent, Belgium, 2004, pp. 168–171.
[33] R. Marqués, J. D. Baena, J. Martel, F. Medina, F. Falcone, M. Sorolla, and F. Martín, "Novel small resonant electromagnetic particles for metamaterial and filter design," in *Proc. Electromagnetics in Advanced Applications Int. Conf.*, Turin, Italy, Sep. 2003, pp. 439–442.
[34] J. D. Baena, R. Marqués, F. Medina, and J. Martel, "Artificial magnetic metamaterial design by using spiral resonators," *Phys. Rev. B, Condens. Matter*, vol. 69, pp. 014 402(1)–014 402(5), 2004.
[35] I. Bahl and P. Bhartia, *Microwave Solid State Circuit Design*. Toronto, ON, Canada: Wiley, 1988.
[36] F. Falcone, F. Martin, J. Bonache, R. Marqués, and M. Sorolla, "Coplanar waveguide structures loaded with split ring resonators," *Microwave Opt. Technol. Lett.*, vol. 40, pp. 3–6, 2004.
[37] Y. Chang and L.-T. Chang, "Simple method for the variational analysis of a generalized N-dielectric-layer transmission line," *Electron. Lett.*, vol. 6, pp. 49–50, Feb. 1970.

Juan Domingo Baena was born in El Puerto de Santa María, Cádiz, Spain, in August 1976. He received the Licenciado degree in physics from the Universidad de Sevilla, Seville, Spain, in 2001, and is currently working toward the Ph.D. degree at the Universidad de Sevilla.

In 1999, he was a Software Programmer with Endesa (providing company of electricity in Spain). In September 2002, he joined the Electronic and Electromagnetism Department, Universidad de Sevilla. His current research interests include analysis, design, and measurement of artificial media with exotic electromagnetic properties (metamaterials).

Mr. Baena was the recipient of a Spanish Ministry of Science and Technology Scholarship.

Jordi Bonache was born in Barcelona, Spain, in 1976. He received the Physics and Electronics Engineering degrees from the Universitat Autònoma de Barcelona, Barcelona, Spain, in 1999 and 2001, respectively, and is currently working toward the Ph.D. degree at the Universitat Autònoma de Barcelona.

In 2000, he joined the High Energy Physics Institute of Barcelona (IFAE), where he was involved in the design and implementation of the control and monitoring system of the MAGIC telescope. In 2001, he joined the Departament d'Enginyeria Electrònica, Universitat Autònoma de Barcelona, where he is currently an Assistant Professor. His research interests include active and passive microwave devices and metamaterials.

Ferran Martín was born in Barakaldo (Vizcaya), Spain, in 1965. He received the B.S. degree in physics and Ph.D. degree from the Universitat Autònoma de Barcelona, Barcelona, Spain, in 1988 and 1992, respectively.

Since 1994, he has been an Associate Professor of electronics with the Departament d'Enginyeria Electrònica, Universitat Autònoma de Barcelona. He has recently been involved in different research activities including modeling and simulation of electron devices for high-frequency applications, millimeter-wave and terahertz generation systems, and the application of electromagnetic bandgaps to microwave and millimeter-wave circuits. He is also currently very active in the field of metamaterials and their application to the miniaturization and optimization of microwave circuits and antennas.

Ricardo Marqués Sillero (M'95) was born in San Fernando (Cádiz), Spain, in 1954. He received the Ph.D. degree from the Universidad de Sevilla, Seville, Spain, in 1987.

He is currently an Associate Professor with the Universidad de Sevilla. Since 1984, he has been with the Microwave Group, Department of Electronics and Electromagnetism, Universidad de Sevilla. His main fields of interest include computer-aided design (CAD) for microwave integrated circuit (MIC) devices, wave propagation in ferrites, and other complex and anisotropic media and field theory. His recent research interest is focused on the analysis and design of artificial media with exotic electromagnetic properties (metametarials), including negative refraction, sub-wavelength focusing, and their applications in microwave technology.

Francisco Falcone was born in Caracas, Venezuela, in 1974. He received the M.Sc. degree in telecommunication engineering from the Public University of Navarre, Navarre, Spain, in 1999, and is currently working toward the Ph.D. degree in telecommunication engineering from the Public University of Navarre.

From 1999 to 2000, he was with the Microwave Implementation Department, Siemens-Italtel, where he was involved with the layout of the Amena mobile operator. Since 2000, he has been a Radio Network Engineer with Telefónica Móviles España. Since the beginning of 2003, he has also been an Associate Lecturer with the Electrical and Electronic Engineering Department, Public University of Navarre. His main research interests include electromagnetic-bandgap devices, periodic structures, and metamaterials.

Txema Lopetegi (S'99–M'03) was born in Pamplona, Navarre, Spain, in 1973. He received the M.Sc. and Ph.D. degrees in telecommunication engineering from the Public University of Navarre, Navarre, Spain, in 1997 and 2002, respectively.

Since 1997, he has been with the Electrical and Electronic Engineering Department, Public University of Navarre, as an Academic Associate from 1997 to 1999, and as an Assistant Professor since 2000. During 2002 and 2003, he was a Post-Doctoral Researcher with the Payload Systems Division, European Space Research and Technology Center (ESTEC), European Space Agency (ESA), Noordwijk, The Netherlands. His current research interests include metamaterials and their applications in microwave and millimeter-wave technologies (electromagnetic-bandgap structures, left-handed media, and SRRs), as well as coupled-mode theory and synthesis techniques using inverse scattering.

Dr. Lopetegi was the recipient of a 1999 and 2000 grant from the Spanish Ministry of Education to support the research of his doctoral thesis.

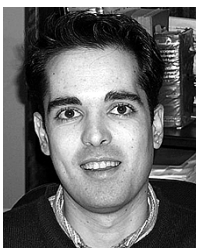

Miguel A. G. Laso (S'99–M'03) was born in Pamplona, Spain, in 1973. He received the M.Sc. and Ph.D. degrees in telecommunication engineering from the Public University of Navarre, Navarre, Spain, in 1997 and 2002, respectively.

Since 2001, he has been an Assistant Lecturer with the Electrical and Electronic Engineering Department, Public University of Navarre. He has been involved in several projects funded by the Spanish Government and the European Union. He was a Post-Doctoral Researcher supported by the Spanish Ministry of Science and Technology with the Payload System Division, European Space Research and Technology Center (ESTEC), European Space Agency (ESA), Noordwijk, The Netherlands, where he was involved with satellite applications of electromagnetic crystals in the microwave range. His current interests include electromagnetic crystals, metamaterials, and periodic structures in planar microwave and millimeter-wave technologies and in the optical wavelength range.

Dr. Laso was the recipient of a grant from the Spanish Ministry of Education to support the research of his doctoral thesis from 1998 to 2002.

Joan Garcia–Garcia was born in Barcelona, Spain in 1971. He received the Physics degree and Ph.D. degree in electrical engineering from the Universitat Autònoma de Barcelona, Barcelona, Spain, in 1994 and 2001, respectively.

He then became a Post-Doctoral Research Fellow with the Institute of Microwaves and Photonics, The University of Leeds, Leeds, U.K., working under the INTERACT European project. In 2002, he was a Post-Doctoral Research Fellow with the Universitat Autònoma de Barcelona, working under the Ramon y Cajal project of the Spanish Government. In November 2003, he become an Associate Professor of electronics with the Departament d'Enginyeria Electrònica, Universitat Autònoma de Barcelona.

Ignacio Gil was born in Barcelona, Spain, in 1978. He received the Physics and Electronics Engineering degrees from the Universitat Autònoma de Barcelona, Barcelona, Spain, in 2000 and 2003, respectively, and is currently working toward the Ph.D. degree at the Universitat Autònoma de Barcelona.

He is also an Assistant Professor with the Universitat Autònoma de Barcelona. His research interests include active and passive microwave devices and metamaterials.

Maria Flores Portillo was born in Pamplona, Spain, in 1980. She received the Telecommunication Engineering degree from the Universidad Pública de Navarra, Navarra, Spain, in 2004.

Her research interests include passive microwave devices and metamaterials.

Mario Sorolla (S'82–M'83–SM'01) was born in Vinaròs, Spain, in 1958. He received the M.Sc. degree from the Polytechnic University of Catalonia, Catalonia, Spain, in 1984, and the Ph.D. degree from the Polytechnic University of Madrid, Madrid, Spain, in 1991, both in telecommunication engineering.

From 1986 to 1990, he designed very high-power millimeter waveguides for plasma heating for the Euratom-Ciemat Spanish Nuclear Fusion Experiment. From 1987 to 1988, he was an Invited Scientist with the Institute of Plasma Research, Stuttgart University, Stuttgart, Germany. He has been involved with MICs and monolithic microwave integrated circuits for satellite communications with Tagra, Les Franqueses del Vallés, Spain, and Mier Communications, Barcelona, Spain. From 1984 to 1986, he was an Assistant Lecturer with the Polytechnic University of Catalonia, Vilanova i la Geltrú, Spain. From 1991 to 1993, he was an Assistant Lecturer with the Ramon Llull University, Barcelona, Spain. From 1993 to 2002, he was an Assistant Professor with the Public University of Navarre, Navarre, Spain, where he is currently a Full Professor with the Electrical and Electronic Engineering Department. His research interest include high-power millimeter waveguide components and antennas, coupled-wave theory, quasi-optical systems in the millimeter and terahertz range, and applications of metamaterials and enhanced transmission phenomena to microwave circuits and antennas.